The Journal of Chemical Physics

RESEARCH ARTICLE | MAY 19 2025

Quantitative relations between nearest-neighbor persistence and slow heterogeneous dynamics in supercooled liquids

Katrianna S. Sarkar ; Kevin A. Interiano-Alberto; Jack F. Douglas ; Robert S. Hoy

J. Chem. Phys. 162, 194502 (2025)
https://doi.org/10.1063/5.0262404
CHORUS

The Journal of Chemical Physics ARTICLE pubs.aip.org/aip/jcp

Quantitative relations between nearest-neighbor persistence and slow heterogeneous dynamics in supercooled liquids

Cite as: J. Chem. Phys. 162, 194502 (2025); doi: 10.1063/5.0262404
Submitted: 1 February 2025 • Accepted: 2 May 2025 •
Published Online: 19 May 2025

Katrianna S. Sarkar,[1] Kevin A. Interiano-Alberto,[1] Jack F. Douglas,[2] and Robert S. Hoy[1,a)]

AFFILIATIONS

[1] Department of Physics, University of South Florida, Tampa, Florida 33620, USA
[2] National Institute of Standards and Technology, Gaithersburg, Maryland 20899, USA

[a)] Author to whom correspondence should be addressed: rshoy@usf.edu

ABSTRACT

Using molecular dynamics simulations of a binary Lennard-Jones model of glass-forming liquids, we examine how the decay of the normalized neighbor-persistence function $C_B(t)$, which decays from unity at short times to zero at long times as particles lose the neighbors that were present in their original first coordination shell, compares with those of other, more conventionally utilized relaxation metrics. In the strongly non-Arrhenius temperature regime below the onset temperature T_A, we find that $C_B(t)$ can be described using the same generic double-stretched-exponential functional form that is often utilized to fit the self-intermediate scattering function $S(q,t)$ of glass-forming liquids in this regime. The ratio of the bond lifetime τ_{bond} associated with $C_B(t)$'s slower decay mode to the α-relaxation time τ_α varies appreciably and non-monotonically with T, peaking at $\tau_{bond}/\tau_\alpha \simeq 45$ at $T \simeq T_x$, where T_x is a crossover temperature separating the high- and low-temperature regimes of glass-formation. In contrast, τ_{bond} remains on the order of the overlap time τ_{ov} (the time interval over which a typical particle moves by half its diameter), and the peak time τ_χ for the susceptibility $\chi_B(t)$ associated with the spatial heterogeneity of $C_B(t)$ remains on the order of τ_{imm} (the characteristic lifetime of immobile-particle clusters), even as each of these quantities varies by roughly 5 orders of magnitude over our studied range of T. Thus, we show that $C_B(t)$ and $\chi_B(t)$ provide semi-quantitative spatially-averaged measures of the slow heterogeneous dynamics associated with the persistence of immobile-particle clusters.

I. INTRODUCTION

Numerous experimental and computational studies have shown that glass-forming liquids are dynamically heterogeneous, in the sense that they possess transient regions where the relaxation dynamics can be substantially faster or slower than their spatial average.[1–14] High-mobility particles tend to form clusters with lifetimes scaling as $\tau_{mob} \sim T/D$, where T is the temperature and D is the diffusion constant. Low-mobility particles tend to form clusters with lifetimes $\tau_{imm} \sim \tau_\alpha$, where τ_α is the α-relaxation time. Most studies of dynamical heterogeneity have focused on the mobile-particle clusters, and the associated cooperative motion of the mobile particles, in relation to understanding glass-forming liquids' temperature-dependent activation energy $E_A(T)$.

Immobile-particle clusters have also been shown to play a significant role in these liquids' dramatic dynamical slowdown. Lačević *et al.* connected these clusters directly to α relaxation more than twenty years ago[10] by showing that they dominate the four-point position-time susceptibility $\chi_4(t)$ and that the time $\tau_{4,pos}$ at which $\chi_4(t)$ is maximized tracks τ_α with decreasing T. Many studies performed since then have *defined* "dynamical heterogeneity" (DH) in terms of $\chi_4(t)$. DH has also been often defined in terms of the more easily calculated and experimentally determined peak in the non-Gaussian parameter $\alpha_2(t)$. Notably, the time t^* at which α_2 is maximized is a "slow β" relaxation time in the sense that it is much longer than the fast β relaxation time τ_β governing the initial decay of $S(q,t)$, but much shorter than τ_α, in glass-forming liquids at low temperatures. Recent work has shown that the T-dependence of t^* closely tracks that of the Johari–Goldstein relaxation time τ_{JG}.[15,16]

Starr *et al.* showed[11] that there are two distinct types of dynamic heterogeneity on these time scales [i.e., $\mathcal{O}(t^*)$ and $\mathcal{O}(\tau_\alpha)$], which are, respectively, associated with the mobile- and immobile-particle

clusters; below, we refer to these as "fast" and "slow" DH. However, despite the advances made by a few more-recent studies,[17–20] immobile-particle clusters and slow DH remain relatively poorly studied in comparison to their mobile-particle and fast counterparts, and there is clearly a need to better understand these phenomena.

In this paper, we take a different approach to characterizing the spatially heterogeneous dynamics associated with the immobile-particle clusters. In particular, we focus on the neighbor-persistence metric $C_B(t)$, which varies smoothly from 1 to 0 as particles lose the neighbors that were present in their original first coordination shell, and captures the extent to which individual particles progressively "forget" their original local environments. $C_B(t)$ was suggested to be a natural measure of structural relaxation in supercooled liquids as far back as the work of Frenkel in the 1930s,[21] and Rahman examined related quantities in some of the first molecular dynamics simulations,[22] yet this metric has received surprisingly little attention over the intervening decades. This neglect can no doubt be traced to the fact that it cannot yet be experimentally measured in atomic and molecular glass-formers.

Experimental measurements of $C_B(t)$ have, however, been performed for *colloidal* glass-formers. Conrad *et al.* showed that their solid-like, elastic response to an applied shear strain on timescales $t < \tau_{solid}$ arises from the system-spanning nature of the immobile-particle clusters on these timescales.[23] They showed that these clusters have $C_B(t < \tau_{solid}) = 1$, and further, that in the glassy state, such clusters persist throughout the experimental observation window. Zhang *et al.* compared $C_B(t)$ in attractive and repulsive glasses composed of the same particles at the same packing fractions[24] and showed that the much-slower dynamics of the former systems is directly associated with their much-slower-decaying $C_B(t)$. Laurati *et al.* extended the results of Ref. 23 to mechanically deformed systems, showing[25] that the shape of the stress–strain curves $\sigma(\gamma)$ under startup shear is intimately connected to $C_B(\gamma)$, i.e., to the fraction of particles' neighbors in the initial undeformed state that remain their neighbors at shear strain γ. Most recently, Higler *et al.* measured $C_B(t)$ in charge-stabilized colloidal suspensions with a wide range of ϕ, τ_α, τ_{bond}, and coordination numbers Z.[26] They used these results to reformulate Dyre's shoving model[27,28] for the relationship between τ_α and the cage-escape lifetime τ_{cage} (which is of order τ_{bond}) in terms of more-readily observable particle-scale quantities.

Several additional insights have come from molecular dynamics simulations. Yamamoto and Onuki showed[29] that the time scale τ_{bond} associated with the decay of $C_B(t)$ at large t seemed to satisfy the relation $\tau_{bond} \simeq 10\tau_\alpha$, that reneighboring events become increasingly spatially heterogeneous with decreasing T, that $\tau_{bond} \propto \xi^z$ where ξ is the correlation length of such heterogeneities (i.e., the size of clusters formed by particles with few lost neighbors), and that the character of these heterogeneities is strongly affected by applied shear. Shiba *et al.* substantially extended these results, showing[30] that $\tau_{4,pos}$ was considerably shorter than the peak time $\tau_{4,bond}$ for four-point bond-breakage correlations, and claimed that this is associated with long-wavelength vibrational modes, which reduce the former but not the latter. Iwashita *et al.* argued[31] that $C_B(t)$ is directly connected to the super-Arrhenius temperature dependence of fragile glassformers' relaxation dynamics. In particular, they identified the average time for particles to lose *one* neighbor (τ_{LC}) as the time scale most directly associated with the elementary excitations in weakly supercooled liquids. Most recently, Scalliet *et al.* compared the spatially resolved $C_B[\tau_{bond}(T)]$ of supercooled liquids over a wide range of T.[32] They showed that the spatial heterogeneity of neighbor persistence increases dramatically as T decreases into a regime that is more deeply supercooled than that probed by most previous simulations. In this regime, structural relaxation corresponds to transient but long-lived solid-like regions with low particle mobility and high C_B being gradually "dissolved" by liquid-like regions displaying opposite trends. This interpretation seems to agree with a wide range of recent theoretical work.[20,33]

Taken together, these results indicate that $C_B(t)$ is an appealing relaxation metric to study because it is both experimentally accessible and simple to interpret, yet it can offer deep insights not obtainable via more-commonly studied metrics such as particles' mean-squared displacement $\Delta^2(t)$ and self-intermediate scattering function $S(q,t)$. However, the *quantitative* relationships between the relaxation times associated with $C_B(t)$ and several other, more-conventionally utilized relaxation metrics have yet to be established. In this paper, using molecular dynamics simulations of the Kob–Andersen (KA) model,[34,35] a model glass-former that has been intensively studied for three decades, we do so.

We find that for temperatures below T_A, where T_A is defined as the temperature below which $\tau_\alpha(T)$ significantly exceeds the value predicted from an Arrhenius fit to the $\tau_\alpha(T)$ for $T > T_A$,[35] $C_B(t)$ is well fit by the same generic double-stretched-exponential functional form

$$C_B(t) = (1-A)\exp\left[-(t/\tau_{fast})^{s_{fast}}\right] + A\ \exp\left[(-t/\tau_{slow})^{s_{slow}}\right] \quad (1)$$

that is often utilized to fit $S(q,t)$ in this regime.[19] Here the notation used in Eq. (1) is chosen to emphasize that this is a very general functional form that is designed to separate "fast" from "slow" relaxation mechanisms. The τ_{fast}, s_{fast}, and s_{slow} we obtain for $C_B(t)$ are close to those obtained by fitting the corresponding fast-β and α relaxation processes of $S(q,t)$, but the $A(T)$ are somewhat larger. Consistent with previous studies,[23–26,29–32] the characteristic neighbor lifetime τ_{slow} is much longer than τ_α. We also find that the ratio τ_{slow}/τ_α varies substantially with T and peaks near T_x, where T_x is a crossover temperature separating the high- and low-temperature regimes of glass-formation.[35–37] On the other hand, τ_{slow} remains within a factor of order one of τ_{ov}, and τ_χ remains within a factor of order one of τ_{imm}, even as each of these quantities varies by roughly 5 orders of magnitude over our studied range of T. Van Hove correlation functions evaluated at $t = \tau_\chi(T)$ reveal that diffusion remains strongly non-Gaussian on this timescale—increasingly so as T decreases—owing to the persistence of large immobile-particle clusters. Thus, we show that $C_B(t)$ and $\chi_B(t)$ provide easily measurable, semi-quantitative, spatially averaged measures of the slow heterogeneous dynamics associated with immobile particles.

II. METHODS

All simulations were conducted using the High Dimensional Molecular Dynamics (`hdMD`) code.[38,39] To capture generic supercooled-liquid behavior, we simulate the standard Kob–Andersen model[34] with a 2:1 ratio of large (A) to small (B) particles. Particles i and j interact via the truncated and shifted Lennard-Jones potential $U(r) = U_{LJ}(r) - U_{LJ}(r_c)$, where

$$U_{\rm LJ}(r) = 4\epsilon_{ij}\left[\left(\frac{\sigma_{ij}}{r}\right)^{12} - \left(\frac{\sigma_{ij}}{r}\right)^{6}\right]. \quad (2)$$

As usual,[34,35] $\epsilon_{\rm AA} = 1.0$, $\epsilon_{\rm AB} = 1.5$, $\epsilon_{\rm BB} = 0.5$, $\sigma_{\rm AA} = 1.0$, $\sigma_{\rm AB} = 0.8$, and $\sigma_{\rm BB} = 0.88$ in units of the system's characteristic energy and length scales, and the cutoff radius $r_c = 2.5\sigma_{\rm ij}$.

Here, we focus on liquids in three spatial dimensions, with periodic boundary conditions applied along each direction of cubic simulation cells. We employ the 2:1 variant of the KA model rather than the historically-more-widely-studied 4:1 variant because the latter is prone to crystallization.[40] All results reported below will be given in units of $\epsilon_{\rm AA}$, $\sigma_{\rm AA}$, and the time scale $\tau = \sqrt{m\sigma_{\rm AA}^2/\epsilon_{\rm AA}}$, where all particles have mass m. The MD time step we employed is $dt = \tau/125$. All systems contain $N = 1.67 \times 10^5$ particles and are equilibrated at various constant temperatures $0.38 \leq T \leq 1.0$ and a small positive pressure $P = 0.01$. In real units corresponding to liquid argon, this pressure corresponds to $P \simeq 420$ kPa, while our highest temperature corresponds to $T \simeq 120$ K.[41,42] As is standard practice,[35] we equilibrate systems for at least $100\tau_\alpha$ [defined using the standard criterion $S(q, \tau_\alpha) = 1/e$] for each T before beginning the measurements reported below.

Following Refs. 23–26 and 29–32, we define $C_B^i(t)$ as the average fraction of neighbors present in particle i's original first coordination shell that are still present at time t. Then $C_{\rm B}(t) = \langle C_B^i(t)\rangle$ is the average of this quantity over all particles, and the susceptibility $\chi_{\rm B}(t) = \sqrt{\langle [C_B^i(t)]^2\rangle - C_{\rm B}(t)^2}$ captures the heterogeneity of this metric. Previous studies of this quantity have defined $C_B^i(t)$ as the average fraction of particle pairs with $r_{ij}(0) \leq B_1\sigma_{ij}$ that also have $r_{ij}(t) \leq B_2\sigma_{ij}$, where B_1 was set to approximately correspond to the first minimum of the pair correlation functions $g_{ij}(r)$, and $B_2 \simeq 1.2B_1$. Here, particles i and j are considered neighbors at time t if $r_{ij}(t) \leq (5/4)2^{1/6}\sigma_{ij} \simeq 1.4\sigma_{ij}$ for *arbitrary* t; this effectively sets $B_2 = B_1$.

We will compare the relaxation captured by $C_{\rm B}(t)$ and $\chi_{\rm B}(t)$ to several other more-conventionally utilized relaxation metrics, specifically:

- the mean-squared displacement $\Delta^2(t) = \langle|\vec{r}_i(t) - \vec{r}_i(0)|^2\rangle$ and non-Gaussian parameter $\alpha_2(t) = 3\langle|\vec{r}_i(t) - \vec{r}_i(0)|^4\rangle/(5[\Delta^2(t)]^2) - 1$;[2,35]
- the self-intermediate scattering function $S(q,t)$, averaged over the range $7.55 \leq q \leq 7.75$, i.e., overall q values that are within $0.1/\sigma_{\rm AA}$ of the peak of the static structure factor $S(q)$ for $T \simeq T_{\rm x}$;
- the overlap function $f_{\rm ov}(t)$,[10] here defined as the fraction of particles that remain within $\sigma_{ii}/2$ of their initial positions;
- the average sizes $N_{\rm mob}(t)$ and $N_{\rm imm}(t)$ of mobile- and immobile-particle clusters;[7–11] and
- the self-part of the van Hove correlation function $G_s(r,t) = N^{-1}\sum_{i=1}^{N}\delta(|\vec{r}_i(t) - \vec{r}_i(0)| - r)$,[35] where δ(x) is the Dirac delta function.

To obtain a relatively simple theoretical picture, it is necessary to extract characteristic timescales from the above relaxation metrics. Here, following previous studies,[7–11] we define the times t^*, $\tau_{\rm mob}$, and $\tau_{\rm imm}$ as the peak times for $\alpha_2(t)$, $N_{\rm mob}(t)$, and $N_{\rm imm}(t)$, and similarly, we define the time τ_χ as the peak time for $\chi_{\rm B}(t)$. Results for all of these quantities are time-averaged over at least ten "windows" of length $10^4\tau$ for $T > 0.42$, six windows of length $10^5\tau$ $(2.5 \times 10^5\tau)$ for $0.41 \leq T \leq 0.42$ $(0.39 \leq T \leq 0.40)$, and three windows of length $5 \times 10^5\tau$ for $T = 0.38$.

Rigorously characterizing particles as "mobile" or "immobile" is a non-trivial exercise. Here, we defined the mobile (immobile) particles as the 10% of particles that had the largest (smallest) *maximal* excursions from their initial positions over the time interval $[0, t]$. As in Ref. 43, this percentage was chosen because it maximized the peak *normalized* average mobile-particle cluster size, i.e., the maximal $N_{\rm mob}(t)/N_{\rm rand}$, where $N_{\rm rand}$ is the average size of clusters formed by randomly selected particles.

Note that the $f_{\rm ov}(t)$ defined above is the *self*-overlap function, i.e.,

$$f_{\rm ov}^{\rm self}(t) = \frac{1}{N}\sum_{i=1}^{N}\Theta[\sigma_{ii}/2 - |\vec{r}_i(t) - \vec{r}_i(0)|], \quad (3)$$

where Θ is the Heaviside step function. Reference 10 showed that the abovementioned four-point susceptibility $\chi_4(t) = \frac{V}{Nk_{\rm B}T}(\langle[f_{\rm ov}^{\rm mut}(t)]^2\rangle - \langle f_{\rm ov}^{\rm mut}(t)\rangle^2)$, where the *mutual* overlap function $f_{\rm ov}^{\rm mut}(t)$ given by

$$f_{\rm ov}^{\rm mut}(t) = \frac{1}{N}\sum_{i=1}^{N}\sum_{j=1}^{N}\Theta[a\sigma_{ij} - |\vec{r}_j(t) - \vec{r}_i(0)|] \quad (4)$$

is equal to the integral of the four-point position/time correlation function $\mathcal{G}[\vec{r}_i(0), \vec{r}_j(t), \vec{r}_k(0), \vec{r}_l(t)]$ over all $[\vec{r}_i(0), \vec{r}_j(t), \vec{r}_k(0), \vec{r}_l(t)]$. It also showed that $f_{\rm ov}^{\rm self}(t)$ provides the dominant contribution to $f_{\rm ov}^{\rm mut}(t)$, and that choosing $a = 0.3$ maximizes the heights $\chi_4^{\rm max}(T)$ of the peaks of $\chi_4(t)$. Many studies that have used this cutoff have *defined* DH in terms of $\chi_4(t)$. Moreover, it has been argued that $\chi_4^{\rm max}(T)$ scales with the characteristic correlation lengths $\xi_4(T)$ of DH over time scales $t \sim \tau_\alpha$ as $\chi_4^{\rm max} \sim \xi_4^{2-\varepsilon}$, where the scaling exponent is material-dependent.[44–47] Below, we will show that our alternative choice (i.e., $a = 1/2$) allows us to more effectively characterize systems' slow DH on time scales $t \gg \tau_\alpha$.

III. RESULTS

A. Qualitative characterization of eight different structural-relaxation metrics

Figure 1 summarizes the T- and t-dependence for five of the metrics discussed above. All results shown in panels 1(a) and 1(b) are similar to those reported in many previous studies,[1,35] but since they set the stage for what will follow, we discuss them in some detail here. Plateaus in both $\Delta^2(t)$ and $S(q,t)$ begin to form as T drops below the onset temperature for non-Arrhenius relaxation, $T_{\rm A} \simeq 0.64$; this corresponds to the emergence of a distinct fast β relaxation process with a nearly T-independent relaxation time τ_β and a slow α relaxation process with a strongly T-dependent τ_α. The separation between these timescales upon further cooling exhibits a sharp increase as T drops below $T_{\rm x} \simeq 0.45$. We will discuss how these estimates of $T_{\rm A}$ and $T_{\rm x}$ were obtained in Sec. III B.

There are two notable differences between the behavior of $\Delta^2(t)$ and $S(q,t)$ and that of $f_{\rm ov}(t)$ [panel 1(c)]. First, unlike the former metrics, $f_{\rm ov}(t)$ exhibits single-step decay for all T. Second,

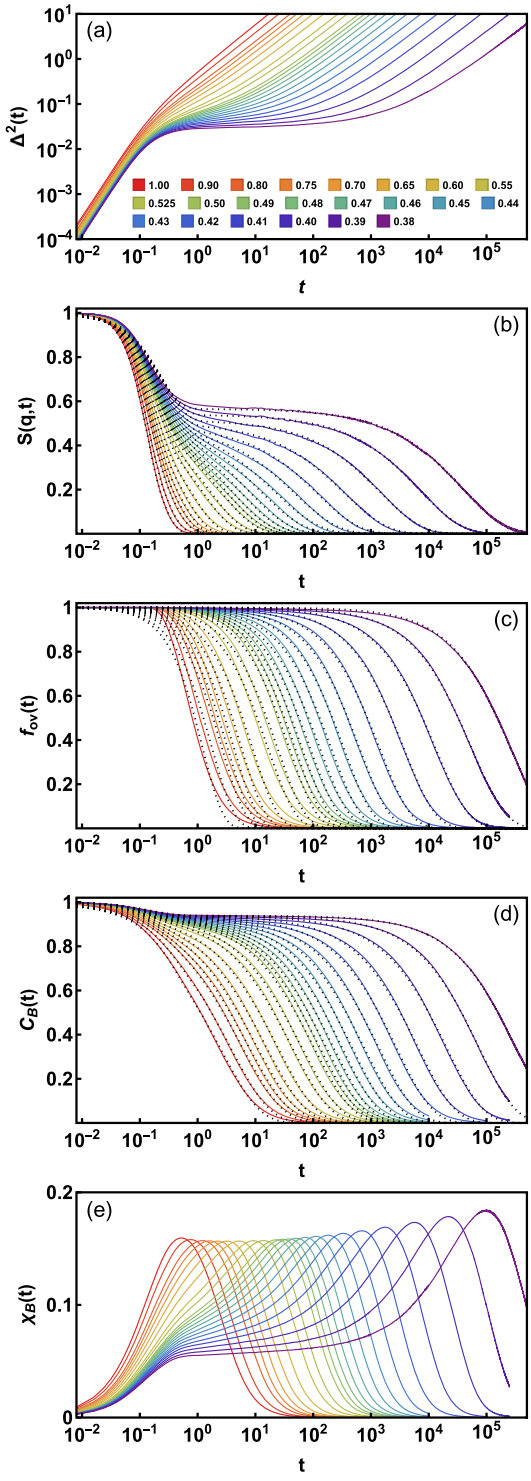

FIG. 1. Three traditional measures of single-particle dynamics compared to two measures of nearest-neighbor persistence. Panels (a)–(e), respectively, show $\Delta^2(t)$, $S(q,t)$, $f_{ov}(t)$, $C_B(t)$, and $\chi_B(t)$ for systems over the temperature range $0.38 \le T \le 1.0$. The color legend in panel (a) shows each T value. Dotted curves in panels (b)–(d) show fits to Eqs. (5)–(7).

in contrast to previous studies that employed $a = 0.3$ (Sec. II) and found that the characteristic relaxation time τ_{ov} defined by $f_{ov}(\tau_{ov}) = 1/e$ was of order τ_α, the plateaus in $f_{ov}(t)$ shown here extend to considerably longer times, indicating $\tau_{ov} \gg \tau_\alpha$. In other words, throughout the plateau regimes suggested by the measurement of particles' mean-squared displacement and self-intermediate scattering function, very few particles have moved by even half their diameter. This is not surprising given that the cage radius $r_{cage} \ll \sigma_{ii}/2$, but it does raise the question of how to visualize the physical relaxation process associated with these larger τ_{ov}.

To begin answering this question, we now look at these systems' $C_B(t)$ [panel 1(d)]. At high and intermediate T, the $C_B(t)$ exhibits smooth, apparently single-timescale decays similar to those reported in previous studies.[23–26,29–32] For $T \lesssim T_x$, however, the $C_B(t)$ exhibits plateaus that lengthen rapidly with decreasing T, much like those shown for $\Delta^2(t)$, $S(q,t)$, and $f_{ov}(t)$. These plateaus have not been previously reported because Refs. 23–26 and 29–32 employed B_2 values, which were well above B_1 (Sec. II), whereas here we employ $B_2 = B_1$. This difference introduces an additional relaxation mechanism in our $C_B(t)$ that was not captured in previous studies: in particular, particle-pair distances evolving back and forth across the above-mentioned $r_{ij} \le (5/4)2^{1/6}\sigma_{ij}$ neighboring cutoff. Below, we will argue that this mechanism is associated with fast β relaxation.

Beyond their plateau regimes, the decays of $C_B(t)$ and $f_{ov}(t)$ closely track each other, indicating that particles losing their neighbors roughly correspond to them moving by more than half their diameters. This is not surprising from a qualitative point of view, but as we will show below, it leads to an interpretation of the connection of $C_B(t)$ to other measures of heterogeneous relaxation dynamics that is substantially different from those developed in previous studies that employed $a = 0.3$.[10,29,30] Note that panels 1(b)–1(d) also show fits of $S(q,t)$, $f_{ov}(t)$, and $C_B(t)$ to Eq. (1), but before discussing these, we will turn our attention to measures of heterogeneous dynamics in these systems.

At the same high T for which $S(q,t)$ and $C_B(t)$ exhibit single-timescale relaxation, $\chi_B(t)$ takes on an approximately log-normal form [panel 1(e)]. As T drops below T_x, clear plateaus of $\chi_B(t)$ that mirror those of $C_B(t)$ emerge. Beyond the plateau regime, the heights $\chi_B^{max}(T)$ of the peaks in the $\chi_B(t)$ curves begin increasing with decreasing T; this is consistent with the increasing contrast between high-$C_B(\tau_{bond})$ and low-$C_B(\tau_{bond})$ regions reported in Ref. 32. Also note that the gradual emergence of two-timescale decay of $S(q,t)$ and $C_B(t)$, as T decreases, coincides with (1) a decrease in the maximal slopes $d\chi_B/d[\ln(t)]$, (2) a reduction of the χ_B values at which the inflection points in the $\chi_B(t)$ curves occur, and (3) a rapid increase in τ_χ. All of these trends indicate that $C_B(t)$ and $\chi_B(t)$, as defined in this paper, can serve as useful *spatially averaged* measures of the slow DH associated with the relatively immobile particles.

Figure 2 shows results for three more metrics that are often employed to characterize dynamical heterogeneity. In all panels, the trends with decreasing T are consistent with many previous studies.[7–11] More specifically, the maximum values of $\alpha_2(t)$, $N_{mob}(t)$, and $N_{imm}(t)$, and the times t^*, τ_{mob}, and τ_{imm} at which these maxima occur, each increase rapidly with decreasing T for $T \lesssim T_x$. The increasing separation between fast DH timescales such as t^* and τ_{mob} and slow DH timescales such as τ_{imm} has been discussed extensively.[1–3,11] However, as mentioned in the Introduction, while most previous studies have focused on assigning a

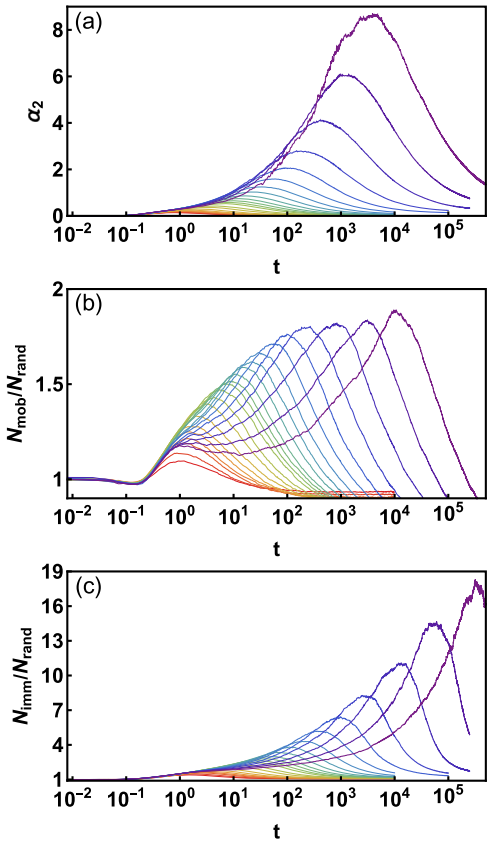

FIG. 2. Traditional measures of dynamical heterogeneity. Panels (a)–(c), respectively, show $\alpha_2(t)$, $N_{mob}(t)$, and $N_{imm}(t)$ for all systems. Colors are the same as in Fig. 1.

physical meaning to the fast timescales (e.g., showing that $t^* \sim \tau_{mob} \sim T/D$[7–11]), here we will focus on the relatively slow particles. More specifically, we will quantitatively relate τ_{imm}, which measures the characteristic lifetime of immobile regions whose characteristic size grows very rapidly with increasing T,[10,11] to *local, single-length-scale* neighbor-persistence timescales obtainable from measurements of $C_B(t)$ and $\chi_B(T)$.

B. Quantitative comparison of seven different relaxation times

Next, we fit the data shown in Figs. 1(a)–1(c) to the common, non-exponential functional form discussed above [Eq. (1)]. To avoid ambiguity in the following discussion, we will first rewrite Eq. (1) in ways that are specific to the three quantities of interest. For the self-intermediate scattering function, we rewrite it as[19,48,49]

$$S(q,t) = (1 - A_S)\exp\left[-(t/\tau_\beta)^{s_\beta}\right] + A_S \exp\left[(-t/\tau_\alpha)^{s_\alpha}\right], \quad (5)$$

where A_S is the well-known "non-ergodicity" parameter,[50] τ_β and τ_α are the fast β and α relaxation times, respectively, and s_β and s_α are the associated exponents quantifying the degree of deviation from exponential relaxation.[51–57] This form should accurately describe $S(q,t)$ for temperatures $T < T_A$, where $\tau_\alpha \gg \tau_\beta$.

For the overlap function, the fact that $f_{ov}(t) \equiv 1$ until particles begin moving at least half their diameters away from their initial positions allows us to set $A = 1$, and therefore to reduce the number of parameters in Eq. (1) from five to two. Thus, we rewrite Eq. (1) as

$$f_{ov}(t) \simeq \exp\left[(-t/\tau_{ov})^{s_{ov}}\right], \quad (6)$$

where τ_{ov} is the relaxation time associated with this process and s_{ov} is the associated stretching exponent. The poor agreement of this approximate functional form with simulation results for $t \lesssim 10^0$ [Fig. 1(c)] is not a major concern for the purposes of this study because we are focusing on the terminal relaxation. Note that this issue could have been avoided by using $f_{ov}^{mut}(t)$ [Eq. (4)], which exhibits a two-step decay for $T \lesssim T_x$[10] and can be fit using the same functional form as Eqs. (1) and (5).

Finally, for the neighbor-persistence function, we rewrite Eq. (1) as

$$C_B(t) = (1 - A_C)\exp\left[-(t/\tau_{fast})^{s_{fast}}\right] + A_C \exp\left[(-t/\tau_{bond})^{s_{bond}}\right]. \quad (7)$$

Here, A_C plays a role similar to the non-ergodicity parameter; the fast-relaxation parameters τ_{fast} and s_{fast} capture the behavior of $C_B(t)$'s abovementioned fast decay mode, and the slow-relaxation parameters τ_{bond} and s_{bond} are the average nearest-neighbor lifetime and associated stretching exponent discussed in Refs. 29 and 30. Our best-fit values of the parameters in Eqs. (5)–(7), along with uncertainty estimates, are given in the Appendix.

Before proceeding further, we define both the onset temperature T_A and the crossover temperature T_x. These temperatures are typically estimated using the α relaxation times. T_A has traditionally been defined[35] as the temperature below which τ_α increases super-Arrheniusly with decreasing T and substantial dynamical heterogeneity emerges.[58] A precise criterion was given in Ref. 42, which showed that defining T_A as the highest temperature for which $\tau_\alpha(T)$ is 1% above its high-T Arrhenius fit value allows $\tau_\alpha(T_A)$ to be identified with the "caging onset time" and to serve as a reference time scale for structural relaxation and diffusion.

T_x has traditionally been defined[35] with the critical temperature T_c of mode-coupling theory by fitting $\tau_\alpha(T)$ to its predicted power-law divergence $\tau_\alpha(T) \sim (T_c - T)^{-\gamma}$[59] over a limited temperature range. Values of T_c obtained in this fashion depend strongly on the choice of temperature range over which $\tau_\alpha(T)$ is fit to this functional form,[60,61] however, τ_α does not actually diverge at the fitted T_c. An alternative estimate of the crossover temperature T_x can be obtained by finding the maximum of $d^2[\ln(\tau_\alpha)]/d(1/T)^2$ on a Stickel plot[62] or (roughly equivalently for systems exhibiting a fragile-to-strong crossover[63]) by finding the intersection of the high-T and low-T Arrhenius fits to $\tau_\alpha(T)$.[36] This definition of T_x is comparable to the crossover temperature defined in the Generalized Entropy Theory (GET)[37] that separates the high- and low-temperature regimes of glass formation. Note that the GET also predicts a power-law variation of τ_α over a limited T range and predicts the precise value of this crossover temperature.

Figure 3 shows $\tau_\alpha(T)$ obtained from fitting our $S(q,t)$ data to Eq. (5). The data are consistent with a previous study of the KA model's 2:1 variant at $P = 0$,[64] and all trends are similar to those observed in many previous studies. Here, we emphasize two key features. First, τ_α increases by more than five orders of magnitude (from $\simeq 0.24$ to $\simeq 3.7 \times 10^4$) as T decreases from 1.0 to 0.38. Second,

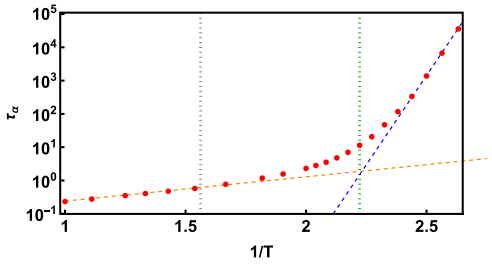

FIG. 3. α relaxation times obtained by fitting $S(q,t)$ to Eq. (5). Dashed lines show fits of $\tau_\alpha(T)$ to the Arrhenius prediction $\tau_{Arr}(T) = \tau_0 \exp(E_{Arr}/T)$; the high- and low-$T$ fits intersect at $T = T_x \simeq 0.45$. The dotted lines indicate $1/T_A$ and $1/T_x$.

the procedures described above[36,42] respectively yield $T_A \simeq 0.64$ and $T_x \simeq 0.45$; for reference, $\tau_\alpha(T_A) \simeq 0.62$ and $\tau_\alpha(T_x) \simeq 12$. Our estimates of T_A and T_x are roughly consistent with the corresponding estimates for the 4:1 KA model when P is small;[42] note that the characteristic temperatures of the Kob–Andersen model depend strongly on pressure,[42] and this should be borne in mind when comparing our results to those from the many previous simulations of the KA model that employed constant density. We will show below that this estimate of T_x closely corresponds to two other distinctive features in the temperature dependence of our systems' relaxation dynamics.

Detailed results for A_S, A_C, τ_β, τ_{fast}, s_β, s_α, s_{ov}, s_{fast}, and s_{bond} are given in the Appendix. Here we emphasize that for all temperatures that are low enough for relaxation to have a distinct two-step character (i.e., $T \leq T_A$), τ_{fast} and s_{fast} are respectively close to τ_β and s_β. This shows that the initial stage of $C_B(t)$'s decay is closely associated with the fast β relaxation.[1] We also find that $s_{bond} \simeq s_\alpha$ for $T \lesssim 0.5$, suggesting that neighbor persistence and α relaxation are similarly heterogeneous in this regime.

Figure 4 shows results for the seven other relaxation times defined above. Panel 4(a) compares the $\tau_\alpha(T)$ obtained by fitting $S(q,t)$ to Eq. (5) to the two measures of fast DH shown in Figs. 2(a) and 2(b). All results are similar to those reported in multiple previous studies.[7–11] The main features we wish to highlight here are that (1) $t^* \simeq \tau_{mob}$ for all but the lowest T, where τ_{mob} is larger; and (2) both t^* and τ_{mob} grow much slower than τ_α with decreasing T.

Panel 4(b) compares these $\tau_\alpha(T)$ to τ_{imm} [Fig. 2(d)], τ_χ, the τ_{ov} obtained by fitting $f_{ov}(t)$ to Eq. (6), and the τ_{bond} obtained by fitting the $C_B(t)$ data to Eq. (7). Three trends are apparent from examining the relations between these quantities. First, as previously reported in Refs. 29–32, τ_α remains well below τ_{bond} for all T. Second, in contrast to the results shown in panel 4(a), τ_α also remains well below the other three timescales for all T, and for high and intermediate temperatures, τ_α grows slower with decreasing T. Third, while τ_{bond} remains on the order of τ_{ov} for all T, τ_{ov} appears to converge to τ_{bond} from below as T decreases. This result is consistent with the geometrically intuitive notion that particles losing their original neighbors correspond to them moving by roughly half their diameter away from their initial positions *when caging is strong and motion is hopping-dominated*, i.e., at low T.

Panels 4(c) and 4(d), which, respectively, show the ratios of τ_{bond} and τ_χ to the other timescales, illustrate the abovementioned

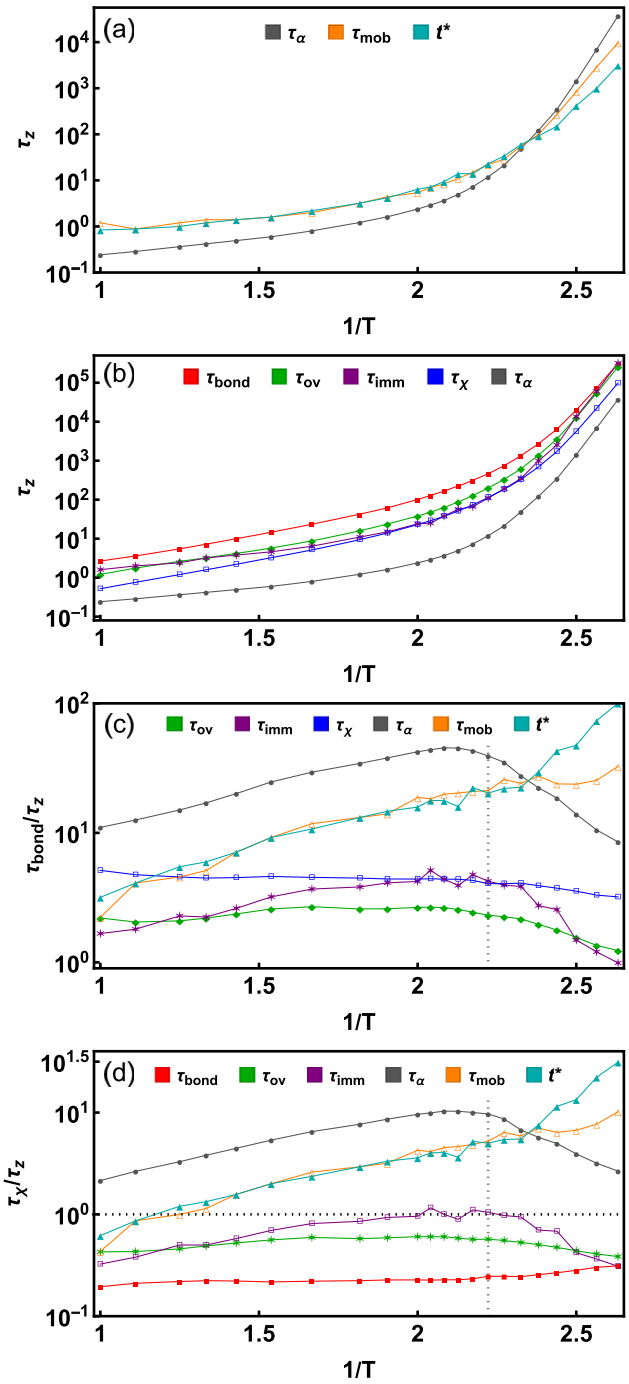

FIG. 4. Comparison of seven different relaxation times τ_z in 2:1 KA liquids at $P = 0.01$. Panels (a) and (b), respectively, compare the relaxation times associated with $C_B(t)$ and $S(q,t)$ to those associated with other metrics for fast and slow DH, while panels (c) and (d), respectively, show the ratios of τ_{bond} and τ_χ to these times. The vertical dotted lines in panels (c) and (d) show $1/T_x$, and the horizontal dotted line in panel (d) shows $\tau_\chi/\tau_z = 1$.

relationships in more detail. Four key trends are apparent. First, the ratios of $\tau_{\rm bond}$ and τ_χ to the fast-DH timescales t^* and $\tau_{\rm mob}$ increase steadily with decreasing T. The ratio of $\tau_{\rm bond}$ to these timescales reaches $\mathcal{O}(10^2)$ at our lowest $T = 0.38$, showing that the much-discussed decoupling[1,2] of the fast and slow relaxation timescales in supercooled liquids also occurs for timescales associated with neighbor persistence. Second, $0.3 < \tau_\chi/\tau_{\rm imm} < 1.2$ and $1.0 < \tau_{\rm bond}/\tau_{\rm imm} < 5.2$ over the entire range of T, even though all three quantities increase by 5 orders of magnitude as T decreases from 1.0 to 0.38. This shows that $C_{\rm B}(t)$ and $\chi_{\rm B}(t)$ are closely associated with the immobile-particle clusters. Third, the ratio $\tau_{\rm bond}/\tau_{\rm ov}$ remains within the very narrow range $2.2 \le \tau_{\rm bond}/\tau_{\rm ov} \le 2.7$ for all $T \ge T_{\rm x}$, but this ratio decreases more rapidly with decreasing T for $T \lesssim T_{\rm x}$, reaching $\simeq 1.2$ at our lowest studied $T = 0.38$.

The fourth trend evident in these panels is that the ratios $\tau_{\rm bond}/\tau_\alpha$ and $\tau_{\rm bond}/\tau_{\rm imm}$ closely track each other, and both appear to peak at $T \simeq 0.48$, which is only slightly above our estimated $T_{\rm x}$. Previous studies have established that $\tau_{\rm imm} \sim \tau_\alpha$.[10,11] We find that the ratio of these two quantities varies over the narrow range $6.5 < \tau_{\rm imm}/\tau_\alpha < 11.5$ despite the fact that each quantity varies by 5 orders of magnitude over our studied range of T. The peaks in $\tau_{\rm bond}/\tau_{\rm imm}$ and $\tau_{\rm bond}/\tau_\alpha$ at $T \simeq T_{\rm x}$ point to a secondary effect that is not captured by the abovementioned connections between $\tau_{\rm bond}$, τ_χ, and $\tau_{\rm imm}$.

Peaks in $\tau_{\rm bond}/\tau_\alpha$ at intermediate T have not been previously reported. They seem inconsistent with Fig. 20 of Ref. 32, which reported $\tau_{\rm bond}/\tau_\alpha$ that decreased monotonically with decreasing T as both quantities varied over a much wider range than is considered here. One plausible explanation for this apparent discrepancy is that our method of estimating $\tau_{\rm bond}$ [i.e., fitting $C_{\rm B}(t)$ to Eq. (7)] separates fast from slow neighbor-decorrelation mechanisms and identifies $\tau_{\rm bond}$ with only the latter. In contrast, previous studies,[23–26,29–32] all of which used $B_2 \simeq 1.2B_1$ and most of which defined $\tau_{\rm bond}$ using the criterion $C_B(\tau_{\rm bond}) = e^{-1}$, did not effectively do so. We found, however, that the peak in $\tau_{\rm bond}/\tau_\alpha$ at $T \simeq T_{\rm x}$ is actually *more* dramatic if we instead define these quantities using $C_B(\tau_{\rm bond}) = e^{-1}$ and $S(q, \tau_\alpha) = e^{-1}$. This issue requires further study, but we emphasize that our results for $T \lesssim T_{\rm x}$ are entirely consistent with those presented in Ref. 32.

We believe that the peaks in $\tau_{\rm bond}/\tau_{\rm imm}$ and $\tau_{\rm bond}/\tau_\alpha$ are directly associated with *decoupling*. Decoupling in an experimental context is often associated with the "breakdown" of the Stokes–Einstein scaling relationship $D \sim \eta^{-1}$ between fluids' mass diffusion coefficient D and shear viscosity η.[1] This breakdown arises when the relatively long timescales associated with the immobile particles and structural relaxation (e.g., τ_χ and τ_α) start growing faster than the shorter timescales associated with the mobile particles and the average rate of molecular diffusion (e.g., $\tau_{\rm mob}$ and t^*) with decreasing T. It is qualitatively described by the "fractional" Stokes–Einstein relation,[65] a general power-law scaling relation $t^* \sim \tau_\alpha^{1-\zeta}$ between these characteristic times, where $\zeta < 1$ is the exponent characterizing the strength of decoupling.[11] Recent work[16,42,66,67] has also connected decoupling directly to τ_β and related this basic molecular timescale to the much longer timescales t^* and τ_α, which are in turn connected directly to the decoupling of D and η. In particular, Yuan *et al.* found that the 4:1 KA model

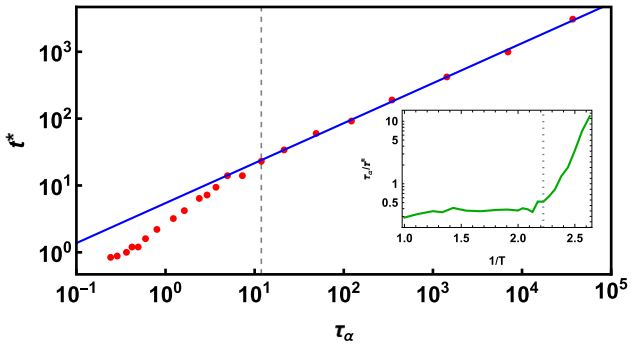

FIG. 5. Coincidence of the peaks in $\tau_{\rm bond}/\tau_\alpha$ and $\tau_{\rm bond}/\tau_{\rm imm}$ with the onset of strong decoupling. The solid line shows a fit of the data to $t^* \sim \tau_\alpha^{1-\zeta}$ (with $\zeta = 0.40$), while the vertical dashed line indicates $\tau_\alpha(T_x)$. In the inset, the curve shows τ_α/t^* for the same dataset shown in Fig. 4, while the vertical dotted line shows $1/T_{\rm x}$.

obeys $t^*/\tau_\beta \sim (\tau_\alpha/\tau_\beta)^{1-\zeta}$, with $\zeta \simeq 0.26$, for a wide range of densities and pressures.[42,67]

As shown in Fig. 5, both the crossover to $t^* \sim \tau_\alpha^{1-\zeta}$ scaling and the onset of rapidly increasing τ_α/t^* occur at $T \simeq T_{\rm x} \simeq 0.45$ in our systems. Thus, the peaks in $\tau_{\rm bond}/\tau_\alpha$ and $\tau_{\rm bond}/\tau_{\rm imm}$, and the subsequent decrease in these quantities with decreasing T, can be interpreted as part of the crossover to the low-temperature ($T < T_{\rm x}$) regime of glass-formation.[37] The $\zeta \simeq 0.40$ value reported here is larger than that reported in Ref. 42 because our measurements of τ_α and t^* were obtained from the $S(q,t)$ and $\alpha_2(t)$ of *all* particles, whereas those performed in Ref. 42 included the dynamics of A particles only, as is the common practice.[35] Adopting this practice for our systems decreases ζ to $\simeq 0.30$ and shifts the crossover to $t^* \sim \tau_\alpha^{1-\zeta}$ scaling upwards, to $T \simeq 0.50$. Here, we prefer to use the values associated with all particles because metrics of heterogeneous dynamics, such as $\tau_{\rm bond}$, $\tau_{\rm mob}$, and $\tau_{\rm imm}$, necessarily include all particles. However, the slightly higher estimate (i.e., $T \simeq 0.50$) is also close to the peaks in $\tau_{\rm bond}/\tau_\alpha$ and $\tau_{\rm bond}/\tau_{\rm imm}$ we find when $C_B(t)$ and $S(q,t)$ are calculated for A particles only. Finally, it must be noted that the P value we have chosen to employ (i.e., $P = 0.01$) is exceptionally low in comparison to most previous studies, and the choice of P apparently influences the point where the power law scaling sets in. This phenomenon requires further study.

C. Connections to heterogeneous caging

Next, we connect the above results to heterogeneous *caging*. In three spatial dimensions, the probability $P(r,t)$ that a particle has moved a distance r away from its initial position after a time t is $P(r,t) = G_s(r,t)/(4\pi r^2)$. According to Einstein's theory of Brownian motion, $P(r,t)$ is Gaussian, and the central limit theorem *requires* that $P(r,t)$ become Gaussian after sufficiently long times for a fluid in thermal equilibrium. At shorter times, however, $P(r,t)$ is distinctly non-Gaussian in a wide variety of glass-forming liquids, including particulate systems near their jamming transitions.[68,69] The slow crossovers to Gaussian $P(r,t)$ have been directly associated[70,71] with the approach to ergodicity.

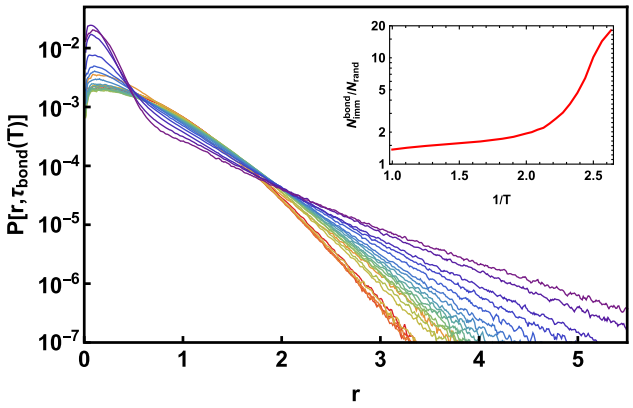

FIG. 6. Normalized van Hove correlation functions evaluated at the $t = \tau_{\text{bond}}(T)$ obtained by fitting $C_{\text{B}}(t)$ to Eq. (7). The inset shows the $N_{\text{imm}}[\tau_{\text{bond}}(T)]/N_{\text{rand}}$ from Fig. 2(c). Colors are the same as in Fig. 1. Note that all trends remain the same if these quantities are instead evaluated at $t = \tau_\chi(T)$.

Exponential tails in $P(r,t)$ taking the form $P_E(r,t) \propto \exp[-r/\Lambda]$, where Λ increases slowly with t,[69–72] have been claimed to be universal in systems where motion is hopping-dominated.[69,72] These tails are known to correspond to the *mobile* particles.[69,72] In contrast, the connection of non-Gaussian $P(r,t)$ on timescales $t \gg \tau_\alpha$ to *immobile* particles and slow DH remains rather poorly characterized. In particular, $P(r,t)$ has not yet been directly related to $C_{\text{B}}(t)$ or the other measures of slow DH discussed above. Here, we do so.

Figure 6 shows that $P[r, \tau_{\text{bond}}(T)]$ becomes increasingly non-Gaussian as T decreases. Two notable trends are evident. First, the lengths of the exponential tails in $P(r)$ increase rapidly with decreasing T for all $T \lesssim T_{\text{A}}$. Since these tails correspond to the mobile particles, this trend reflects the increasing τ_{bond}/t^* and $\tau_{\text{bond}}/\tau_{\text{mob}}$ shown in Fig. 4(c). In other words, the tails correspond to highly mobile particles that have hopped multiple times over the time interval τ_{bond}. Second, a prominent low-r peak develops as T drops below T_{x}. This is directly associated with the above-mentioned increasing peak height of $\chi_{\text{B}}(t)$ [Fig. 1(e)], and more generally, with the increasing spatial contrast between liquid-like mobile and solid-like immobile regions discussed in Ref. 32. The inset shows that it is also directly associated with the persistence of increasingly large immobile-particle clusters. Our results indicate that diffusion does not become fully Gaussian (and ergodicity is not recovered) until t is several times larger than $t = \tau_{\text{bond}}(T)$. While this conclusion is consistent with those of Refs. 23–26 and 29–32, it had not previously been supported so decisively.

To illustrate the connections between the various trends discussed above, Fig. 7 shows snapshots of the largest immobile-particle cluster at $t = \tau_\chi(T)$ for $T = 0.38$. This cluster contains 14 682 atoms, i.e., over 85% of the $N/10$ immobile particles present in the system. It exhibits a fractal structure familiar from previous studies examining the moderately supercooled regime[11,17,32,73] and percolates along all three directions. The left image color-codes particles by their *maximal* displacements Δ_{max} over the interval $0 < t \leq \tau_\chi$, while the right image color-codes particles by their $\mathcal{C}_{\text{B}}^i(\tau_\chi)$. While the two images appear very similar, slightly brighter colors are apparent in the left

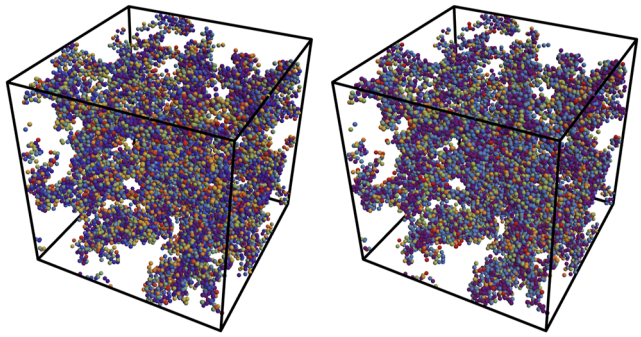

FIG. 7. Snapshots of the largest (14 682-atom) immobile cluster at $t = \tau_\chi(T)$ for $T = 0.38$. Colors vary from purple to red in order of increasing Δ_{max} and in order of decreasing $C_{\text{B}}(\tau_\chi)$.

image, indicating that relatively high-Δ_{max} particles are somewhat more likely than relatively low-$\mathcal{C}_{\text{B}}^i$ particles to be found on the *surface* of the cluster. Note that more than 99% of the atoms in this cluster have $\Delta(\tau_\chi) \equiv \langle|\vec{r}_i(\tau_\chi) - \vec{r}_i(0)|\rangle \leq 0.3$ and $C_{\text{B}}(\tau_\chi) \geq 0.75$, indicating that the low-r peak in $P(r,t)$ (Fig. 6) is dominated by the atoms in this cluster.

IV. DISCUSSION AND CONCLUSIONS

Understanding the dramatic slowdown of supercooled liquids' dynamics with decreasing temperature T is severely hampered by the fact that only a few of the relaxation metrics considered in theories and simulations are readily measurable in experiments. For example, measurements of the diffusion constant D and alpha relaxation time τ_α can be used to investigate characteristic aspects of glassy dynamics such as the breakdown of the Stokes–Einstein relation ($D\tau_\alpha$ = constant),[1,2] and modern probe-molecule-reorientation experiments can provide a great deal of information about dynamical heterogeneity by characterizing how the exponent β associated with stretched-exponential relaxation functions of the common form $F(t) \sim \exp[-(t/\tau)^\beta]$ depends on the length and time scales over which relaxation is probed,[13,14] but such phenomenological observational trends do not provide a clear physical understanding of the molecular origin of these phenomena.

Here, we have shown that a simple neighbor-persistence metric, $C_{\text{B}}(t)$, which *is* readily experimentally accessible in colloidal glassformers,[23–26] can help resolve this issue. In fact, $C_{\text{B}}(t)$ and its variance $\chi_{\text{B}}(t)$ provide near-quantitative metrics for the slow, spatially heterogeneous dynamics that occur over timescales from 10 to $100\tau_\alpha$ and length scales far above those of individual atoms' first coordination shells. More specifically, $C_{\text{B}}(t)$ and $\chi_{\text{B}}(t)$ provide spatially-averaged measures of the dynamics associated with immobile-particle clusters.

We showed that the peak time τ_χ for the susceptibility $\chi_{\text{B}}(t)$ associated with the spatial heterogeneity defined by $C_{\text{B}}(t)$ remains on the order of τ_{imm} (the characteristic lifetime of immobile-particle clusters), even as both of these quantities varied by roughly 5 orders of magnitude over our studied range of T. Examining the Van Hove correlation functions evaluated at $t = \tau_\chi(T)$ reveals that diffusion remains strongly non-Gaussian on this timescale—increasingly so

as T decreases—owing to the persistence of large immobile-particle clusters over this timescale.

Similarly, we showed that the bond lifetime τ_{bond} associated with the terminal decay of $C_B(t)$ remains on the order of the "overlap time" τ_{ov} over which a typical particle moves by at least half its diameter away from its initial position, even as both of these quantities (much like τ_χ and τ_{imm}) varied by roughly 5 orders of magnitude. A key step in making this connection was our decision to use $a = 1/2$ in Eqs. (3) and (4), rather than the smaller value ($a = 0.3$) used in previous studies relating neighbor persistence to heterogeneous dynamics. In particular, choosing $a = 1/2$ made $\tau_{\text{ov}} \simeq \tau_{\text{bond}}$, a relationship that is qualitatively different than the $\tau_{\text{ov}} \simeq \tau_\alpha \ll \tau_{\text{bond}}$ relationship that is observed when $a = 0.3$.[10,29,30]

Finally, we showed that the ratio $\tau_{\text{bond}}/\tau_\alpha$ varies substantially and non-monotonically with T, peaking at $T \simeq T_x$. Recall that τ_α starts to increase sharply, and decoupling of fast and slow relaxation processes occurs, as T drops below the crossover temperature T_x.[1,2] We believe that $\tau_{\text{bond}}/\tau_\alpha$ decreases with decreasing T for $T < T_x$ because the contribution of fast processes to α relaxation diminishes faster with decreasing T than the contribution of these processes to neighbor decorrelation, and hence, τ_α begins growing faster with decreasing T than τ_{bond}. This hypothesis is consistent with Scalliet *et al.*'s data suggesting that $\tau_\alpha \to \tau_{\text{bond}}$ from below as $T \to T_g$[32] and their argument that $\tau_{\text{bond}}/\tau_\alpha$ decreases with decreasing T (for $T < T_x$) because the "coarsening" time scales $\tau_{\text{coarse}} \sim \tau_{\text{bond}}$ over which immobile regions get dissolved from the outside by mobile regions are less strongly T-dependent than τ_α.

How might one further examine the connections between τ_{bond} and other characteristic relaxation times in supercooled liquids? One intriguing possibility suggested in Ref. 32 is that τ_{bond} provides an easily accessible estimate of the "exchange time" τ_{ex},[5,11,13,14,74] which is the average time it takes for a "fast" (high-mobility) region to become "slow" (low-mobility) and vice versa. While τ_{ex} is conceptually straightforward, mapping it onto a specific observable that can be measured in simulations, let alone experiments, has proven challenging.[14] Traditionally, it has been estimated using four-point correlation functions.[29,47,74–76] A recently published study used a novel theoretical approach to calculate τ_{ex} from *two*-point spatiotemporal correlations of local relaxation rates $\gamma(\vec{r}, t)$.[77] It would be very interesting to use this approach to evaluate how $\tau_{\text{bond}}/\tau_{\text{ex}}$ varies with T.

We conclude by summarizing the broader implications of this study for understanding supercooled liquids' dynamics. First, our results demonstrate the limitations of attempting to understand these dynamics using a single relaxation time (e.g., τ_α) or even two characteristic relaxation times (e.g., both τ_α and t^* or τ_{JG}). At the very least, one should also examine a third relaxation time that is substantially larger than τ_α, e.g., τ_{bond} or τ_{ex}. A more fruitful approach, however, may be to focus on the entire *spectrum* for various relaxation processes rather than reducing these to their characteristic time scales.

Second, we showed that τ_{bond} can depend differently on temperature than τ_α *despite* the facts that (i) $C_B(t)$ and $S(q,t)$ can be fit by the same functional form, and (ii) doing so yields $\tau_{\text{fast}} \simeq \tau_\beta$ for $T \lesssim T_A$. Further work is required to obtain a more mechanistic and microscopic understanding of the connections between α relaxation and neighbor decorrelation. Since the most obvious difference between these two processes is that nearby particles moving in the same direction contribute to the former but not the latter, examining the differences between the self and coherent intermediate scattering functions (i.e., comparing how particles diffuse away from their initial *positions* to how they diffuse away from their initial *neighbors*) may shed light on why this is so. Alternatively, one might attempt to relate neighbor decorrelation to the recently discovered "slow Arrhenius process";[78,79] much like τ_{bond}, this process' characteristic relaxation time τ_{SAP} is substantially larger than τ_α at high T but grows slower than τ_α with decreasing T.

ACKNOWLEDGMENTS

We thank Ludovic Berthier and Camille Scalliet for their helpful discussions. This material is based upon work supported by the National Science Foundation under Grant Nos. DMR-2026271 and DMR-2419261.

AUTHOR DECLARATIONS

Conflict of Interest

The authors have no conflicts to disclose.

Author Contributions

Katrianna S. Sarkar: Formal analysis (supporting); Investigation (supporting). **Kevin A. Interiano-Alberto**: Formal analysis (supporting); Investigation (supporting). **Jack F. Douglas**: Conceptualization (equal); Writing – original draft (equal); Writing – review & editing (equal). **Robert S. Hoy**: Conceptualization (equal); Formal analysis (equal); Funding acquisition (equal); Investigation (equal); Supervision (equal); Writing – original draft (equal); Writing – review & editing (equal).

DATA AVAILABILITY

The data that support the findings of this study are available from the corresponding author upon reasonable request.

APPENDIX: QUANTITATIVE DETAILS

Additional results obtained by fitting the $S(q,t)$, $f_{\text{ov}}(t)$, and $C_B(t)$ data to Eqs. (5)–(7) are shown in Fig. 8. Panel 8(a) shows our results for the $A(T)$. Figure 1 had already made it clear that the $A(T)$ are much larger for $C_B(T)$ than they are for $S(q,t)$, but these data show that they are also both nearly T-independent for $T \gtrsim 0.7$. For larger T, these data are less reliable because the nearly single-step nature of the decays of $S(q,t)$ and $C_B(t)$ produces ambiguities in fits of these data to Eqs. (5) and (7).

Panel 8(b) shows that the temperature dependence of the "beta" relaxation times τ_β and τ_{fast} is much weaker than it is for slow timescales such as τ_α and τ_{bond}. This is expected from the well-known weak temperature dependence of β relaxation.[1] In stark contrast to results for the various τ_{slow}, the ratio $\tau_{\text{fast}}/\tau_\beta$ remains nearly constant (and of order one) for all T for which the decay of $S(q,t)$ and $C_B(t)$ clearly has a two-step character, i.e., for all $T \lesssim T_A$. Note that, as mentioned above, in contrast to previous studies,[29–32]

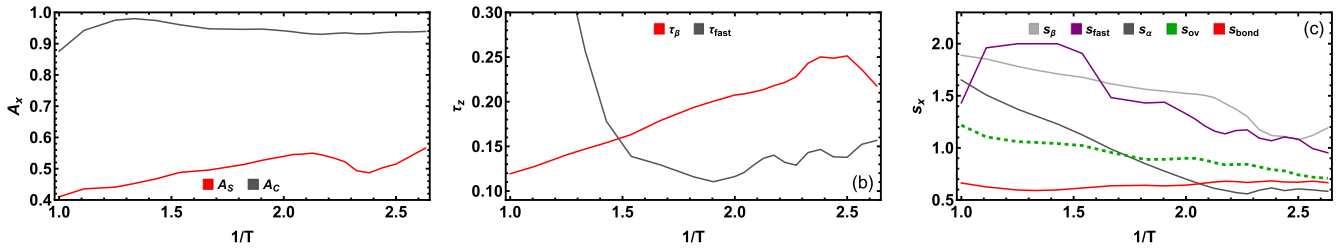

FIG. 8. A_S, A_C, τ_β, τ_{fast}, s_{fast}, s_β, s_{ov}, and s_{bond} values obtained by fitting simulation data for $S(q,t)$, $f_{ov}(t)$, and $C_B(t)$ to Eqs. (5)–(7). Statistical uncertainties for these parameters are comparable to the scatter of the plotted data.

here we did not suppress the fast decay mode of $C_B(t)$ by including a "padding" of the distance cutoff for particles to be considered neighbors.

Panel 8(c) shows our results for the fast and slow stretching exponents. Our results for $s_\beta(T)$ are in qualitative agreement with several previous studies.[52–54] We find that s_{fast} tracks and is comparable to s_β over the entire range of T, further supporting our identification of the fast decay mode of $C_B(t)$ with β relaxation. Since the dynamics of β relaxation are quite complex and remain a topic of active study, it would be interesting to investigate $C_B(t)$'s fast decay mode further, with the aim of explaining how both modes arise from the local event dynamics of the glassy cage.[56,57] We also find that s_{bond} is nearly T-independent; it remains below s_{ov} for all T and is comparable to s_α for $T \lesssim T_x$. α relaxation and neighbor persistence being similarly spatially heterogeneous in this T regime is physically reasonable if both are controlled primarily by the immobile-particle clusters.[11,76] Note that the decrease in s_α with decreasing T is expected to reverse as T drops below T_g;[55–57] it would be very interesting (although computationally expensive) to determine whether this is also true for s_{bond}.

Finally, Table I presents numerical values of the seven relaxation times discussed in Sec. III B. Note that these times are likely to be substantially shorter than the corresponding times in the other recent study of the 2:1 KA model's heterogeneous dynamics at these T[80] because that study employed NVT-ensemble simulations

TABLE I. Equilibrium densities $\rho = N/V$ and best-fit values for the seven relaxation times discussed in Sec. III B. All times are given to two significant figures because the estimated statistical uncertainties on most quantities are of order 1%. The uncertainties for τ_{mob} and τ_{imm} are larger for $T \leq 0.4$ owing to the limited sampling, while those for τ_{mob} and t^* are larger for $T \geq 0.9$ where DH is weak.

T	ρ	τ_{bond}	τ_χ	τ_α	τ_{ov}	τ_{imm}	τ_{mob}	t^*
1	0.933	2.7	0.52	0.24	1.2	1.6	1.2	0.84
0.9	1.016	3.6	0.76	0.29	1.8	2.0	0.88	0.88
0.8	1.085	5.5	1.2	0.37	2.6	2.4	1.2	1.0
0.75	1.116	7.2	1.6	0.42	3.3	3.2	1.4	1.2
0.7	1.147	10	2.2	0.49	4.2	3.8	1.4	1.3
0.65	1.177	15	3.2	0.60	5.7	4.6	1.6	1.6
0.6	1.206	24	5.2	0.80	8.8	6.4	2.0	2.2
0.55	1.235	42	9.4	1.2	16	11	3.2	3.2
0.525	1.248	62	14	1.6	24	15	4.4	4.2
0.5	1.263	1.0×10^2	23	2.4	38	24	5.4	6.4
0.49	1.269	1.3×10^2	29	2.9	48	25	7	7.2
0.48	1.274	1.7×10^2	38	3.7	63	38	8.4	9.4
0.47	1.280	2.2×10^2	51	5.0	87	57	11	13
0.46	1.285	3.1×10^2	73	7.3	1.3×10^2	66	15	15
0.45	1.291	4.7×10^2	1.2×10^2	12	2.0×10^2	1.1×10^2	22	23
0.44	1.297	7.5×10^2	1.9×10^2	21	3.3×10^2	1.9×10^2	29	34
0.43	1.302	1.3×10^3	3.3×10^2	49	6.2×10^2	3.5×10^2	56	60
0.42	1.308	2.7×10^3	7.0×10^2	1.2×10^2	1.4×10^3	9.9×10^2	99	92
0.41	1.314	6.5×10^3	1.7×10^3	3.5×10^2	3.6×10^3	2.5×10^3	2.7×10^2	1.9×10^2
0.4	1.319	2.0×10^4	5.6×10^3	1.4×10^3	1.3×10^4	1.3×10^4	8.4×10^2	4.2×10^2
0.39	1.325	7.3×10^4	2.2×10^4	6.9×10^3	5.4×10^4	6.1×10^4	2.9×10^3	1.0×10^3
0.38	1.330	3.2×10^5	9.9×10^4	3.7×10^4	2.6×10^5	3.2×10^5	9.7×10^3	3.1×10^3

performed at a fixed density $\rho = N/V = 1.4\sigma_{AA}^{-3}$, which is significantly higher than any of the densities considered here. The KA model's dynamics slow down rapidly with increasing pressure, particularly for low P.[42,67]

REFERENCES

[1] M. D. Ediger, C. A. Angell, and S. R. Nagel, "Supercooled liquids and glasses," J. Phys. Chem. **100**, 13200 (1996).
[2] M. D. Ediger, "Spatially heterogeneous dynamics in supercooled liquids," Annu. Rev. Phys. Chem. **51**, 99 (2000).
[3] H. Sillescu, "Heterogeneity at the glass transition: A review," J. Non-Cryst. Solids **243**, 81 (1999).
[4] M. T. Cicerone and M. D. Ediger, "Relaxation of spatially heterogeneous dynamic domains in supercooled ortho-terphenyl," J. Chem. Phys. **103**, 5684 (1995).
[5] A. Heuer, M. Wilhelm, H. Zimmermann, and H. W. Spiess, "Rate memory of structural relaxation in glasses and its detection by multidimensional NMR," Phys. Rev. Lett. **75**, 2851 (1995).
[6] W. K. Kegel and A. van Blaaderen, "Direct observation of dynamical heterogeneities in colloidal hard-sphere suspensions," Science **287**, 290 (2000).
[7] W. Kob, C. Donati, S. J. Plimpton, P. H. Poole, and S. C. Glotzer, "Dynamical heterogeneities in a supercooled Lennard-Jones liquid," Phys. Rev. Lett. **79**, 2827 (1997).
[8] C. Donati, J. F. Douglas, W. Kob, S. J. Plimpton, P. H. Poole, and S. C. Glotzer, "Stringlike cooperative motion in a supercooled liquid," Phys. Rev. Lett. **80**, 2338 (1998).
[9] C. Donati, S. C. Glotzer, P. H. Poole, W. Kob, and S. J. Plimpton, "Spatial correlations of mobility and immobility in a glass-forming Lennard-Jones liquid," Phys. Rev. E **60**, 3107 (1999).
[10] N. Lačević, F. W. Starr, T. B. Schrøder, and S. C. Glotzer, "Spatially heterogeneous dynamics investigated via a time-dependent four-point density correlation function," J. Chem. Phys. **119**, 7372 (2003).
[11] F. W. Starr, J. F. Douglas, and S. Sastry, "The relationship of dynamical heterogeneity to the Adam-Gibbs and random first-order transition theories of glass formation," J. Chem. Phys. **138**, 12A541 (2013).
[12] L. Berthier, G. Biroli, J.-P. Bouchaud, L. Cipeletti, and W. van Saarloos, *Dynamical Heterogeneities in Glasses, Colloids, and Granular Media* (Oxford University Press, 2011).
[13] K. Paeng, H. Park, D. T. Hoang, and L. J. Kaufman, "Ideal probe single-molecule experiments reveal the intrinsic dynamic heterogeneity of a supercooled liquid," Proc. Natl. Acad. Sci. U. S. A. **112**, 4952 (2015).
[14] R. Richert, "Probing liquid dynamics, one molecule at a time," Proc. Natl. Acad. Sci. U. S. A. **112**, 4841 (2015).
[15] F. Puosi, A. Tripodo, M. Malvaldi, and D. Leporini, "Johari–Goldstein heterogeneous dynamics in a model polymer," Macromolecules **54**, 2053 (2021).
[16] X. Xu, J. F. Douglas, and W.-S. Xu, "Thermodynamic–dynamic interrelations in glass-forming polymer fluids," Macromolecules **55**, 8699 (2022).
[17] X. Wang, W.-S. Xu, H. Zhang, and J. F. Douglas, "Universal nature of dynamic heterogeneity in glass-forming liquids: A comparative study of metallic and polymeric glass-forming liquids," J. Chem. Phys. **151**, 184503 (2019).
[18] W. Zhang, J. F. Douglas, and F. W. Starr, "What does the instantaneous normal mode spectrum tell us about dynamical heterogeneity in glass-forming fluids?," J. Chem. Phys. **151**, 184904 (2019).
[19] A. Giuntoli, F. Puosi, D. Leporini, F. W. Starr, and J. F. Douglas, "Predictive relation for the α-relaxation time of a coarse-grained polymer melt under steady shear," Sci. Adv. **6**, eaaz0777 (2020).
[20] L. Gao, H.-B. Yu, T. B. Schrøder, and J. C. Dyre, "Unified percolation scenario for the α and β processes in simple glass formers," Nat. Phys. **21**, 471 (2025).
[21] J. Frenkel, *Kinetic Theory of Liquids* (Oxford University Press, Oxford, 1946).
[22] A. Rahman, "Liquid structure and self-diffusion," J. Chem. Phys. **45**, 2585 (1966).
[23] J. C. Conrad, P. P. Dhillon, E. R. Weeks, D. R. Reichman, and D. A. Weitz, "Contribution of slow clusters to the bulk elasticity near the colloidal glass transition," Phys. Rev. Lett. **97**, 265701 (2006).
[24] Z. Zhang, P. J. Yunker, P. Habdas, and A. G. Yodh, "Cooperative rearrangement regions and dynamical heterogeneities in colloidal glasses with attractive versus repulsive interactions," Phys. Rev. Lett. **107**, 208303 (2011).
[25] M. Laurati, P. Maßhoff, K. J. Mutch, S. U. Egelhaaf, and A. Zaccone, "Long-lived neighbors determine the rheological response of glasses," Phys. Rev. Lett. **118**, 018002 (2017).
[26] R. Higler, J. Krausseer, J. van der Gucht, A. Zaccone, and J. Sprakel, "Linking slow dynamics and microscopic connectivity in suspensions of charged colloids," Soft Matter **14**, 780 (2018).
[27] J. C. Dyre, N. B. Olsen, and T. Christensen, "Local elastic expansion model for viscous-flow activation energies of glass-forming molecular liquids," Phys. Rev. B **53**, 2171 (1996).
[28] J. C. Dyre, "*Colloquium*: The glass transition and elastic models of glass-forming liquids," Rev. Mod. Phys. **78**, 953 (2006).
[29] R. Yamamoto and A. Onuki, "Dynamics of highly supercooled liquids: Heterogeneity, rheology, and diffusion," Phys. Rev. E **58**, 3515 (1998).
[30] H. Shiba, T. Kawasaki, and A. Onuki, "Relationship between bond-breakage correlations and four-point correlations in heterogeneous glassy dynamics: Configuration changes and vibration modes," Phys. Rev. E **86**, 041504 (2012).
[31] T. Iwashita, D. M. Nicholson, and T. Egami, "Elementary excitations and crossover phenomenon in liquids," Phys. Rev. Lett. **110**, 205504 (2013).
[32] C. Scalliet, B. Guiselin, and L. Berthier, "Thirty milliseconds in the life of a supercooled liquid," Phys. Rev. X **12**, 041028 (2022).
[33] J. C. Dyre, "*Solid-that-flows* picture of glass-forming liquids," J. Phys. Chem. Lett. **15**, 1603 (2024).
[34] W. Kob and H. C. Andersen, "Scaling behavior in the beta-relaxation regime of a supercooled Lennard-Jones mixture," Phys. Rev. Lett. **73**, 1376 (1994).
[35] W. Kob and H. C. Andersen, "Testing mode-coupling theory for a supercooled binary Lennard-Jones mixture. II. Intermediate scattering function and dynamic susceptibility," Phys. Rev. E **52**, 4134 (1995).
[36] R. Casalini and C. M. Roland, "Scaling of the supercooled dynamics and its relation to the pressure dependences of the dynamic crossover and the fragility of glass formers," Phys. Rev. B **71**, 014210 (2005).
[37] J. Dudowicz, K. F. Freed, and J. F. Douglas, "Generalized entropy theory of polymer glass formation," Adv. Chem. Phys. **137**, 125 (2008).
[38] R. S. Hoy and K. A. Interiano-Alberto, "Efficient *d*-dimensional molecular dynamics simulations for studies of the glass-jamming transition," Phys. Rev. E **105**, 055305 (2022).
[39] See http://labs.cas.usf.edu/softmattertheory/hdMD.html for the C++ source code and instructions for compiling and running hdMD.
[40] T. S. Ingebrigtsen, J. C. Dyre, T. B. Schrøder, and C. P. Royall, "Crystallization instability in glass-forming mixtures," Phys. Rev. X **9**, 031016 (2019).
[41] S. Sastry, "The relationship between fragility, configurational entropy and the potential energy landscape of glass-forming liquids," Nature **409**, 164 (2001).
[42] Q.-L. Yuan, X. Xu, J. F. Douglas, and W.-S. Xu, "Influence of density and pressure on glass formation in the Kob–Andersen model," J. Phys. Chem. B **128**, 9889 (2024).
[43] X. Wang, H. Zhang, and J. F. Douglas, "The initiation of shear band formation in deformed metallic glasses from soft localized domains," J. Chem. Phys. **155**, 204504 (2021).
[44] S. Karmakar, C. Dasgupta, and S. Sastry, "Growing length and time scales in glass-forming liquids," Proc. Natl. Acad. Sci. U. S. A. **106**, 3675 (2009).
[45] S. Karmakar, C. Dasgupta, and S. Sastry, "Analysis of dynamic heterogeneity in a glass former from the spatial correlations of mobility," Phys. Rev. Lett. **105**, 015701 (2010).
[46] E. Flenner and G. Szamel, "Dynamic heterogeneity in a glass forming fluid: Susceptibility, structure factor, and correlation length," Phys. Rev. Lett. **105**, 217801 (2010).
[47] K. Kim and S. Saito, "Multiple length and time scales of dynamic heterogeneities in model glass-forming liquids: A systematic analysis of multi-point and multi-time correlations," J. Chem. Phys. **138**, 12A506 (2013).
[48] D. S. Simmons and J. F. Douglas, "Nature and interrelations of fast dynamic properties in a coarse-grained glass-forming polymer melt," Soft Matter **7**, 11010 (2011).

[49]W. Zhang, J. F. Douglas, and F. W. Starr, "Effects of a 'bound' substrate layer on the dynamics of supported polymer films," J. Chem. Phys. **147**, 044901 (2017).
[50]R. D. Mountain and D. Thirumalai, "Relationship between the fluctuation metric and the non-ergodicity parameter: Incoherent scattering function," Physica A **192**, 543 (1993).
[51]G. H. Vineyard, "Scattering of slow neutrons by a liquid," Phys. Rev. **110**, 999 (1958).
[52]P. Allegrini, J. F. Douglas, and S. C. Glotzer, "Dynamic entropy as a measure of caging and persistent particle motion in supercooled liquids," Phys. Rev. E **60**, 5714 (1999).
[53]B. A. Pazmiño Betancourt, F. W. Starr, and J. F. Douglas, "String-like collective motion in the α- and β-relaxation of a coarse-grained polymer melt," J. Chem. Phys. **148**, 104508 (2018).
[54]H. Zhang, X. Wang, H.-B. Yu, and J.-F. Douglas, "Fast dynamics in a model metallic glass-forming material," J. Chem. Phys. **154**, 084505 (2021).
[55]B. Ruta, Y. Chushkin, G. Monaco, L. Cipelletti, E. Pineda, P. Bruna, V. M. Giordano, and M. Gonzalez-Silveira, "Atomic-scale relaxation dynamics and aging in a metallic glass probed by X-ray photon correlation spectroscopy," Phys. Rev. Lett. **109**, 165701 (2012).
[56]K. Trachenko and A. Zaccone, "Slow stretched-exponential and fast compressed-exponential relaxation from local event dynamics," J. Phys.: Condens. Matter **33**, 315101 (2021).
[57]V. V. Ginzburg, O. V. Gendelman, and A. Zaccone, "Unifying physical framework for stretched-exponential, compressed-exponential, and logarithmic relaxation phenomena in glassy polymers," Macromolecules **57**, 2520 (2024).
[58]S. Sastry, P. G. Debenedetti, and F. H. Stillinger, "Signatures of distinct dynamical regimes in the energy landscape of a glass-forming liquid," Nature **393**, 554 (1998).
[59]U. Bengtzelius, W. Gotze, and A. Sjolander, "Dynamics of supercooled liquids and the glass transition," J. Phys. C: Solid State Phys. **17**, 5915 (1984).
[60]L. Berthier and G. Tarjus, "Critical test of the mode-coupling theory of the glass transition," Phys. Rev. E **82**, 031502 (2010).
[61]J.-H. Hung and D. S. Simmons, "Does the naive mode-coupling power law divergence provide an objective determination of the crossover temperature in glass formation behavior?," J. Phys. Chem. B **129**, 3018 (2025).
[62]F. Stickel, E. W. Fischer, and R. Richert, "Dynamics of glass-forming liquids. II. Detailed comparison of dielectric relaxation, dc-conductivity, and viscosity data," J. Chem. Phys. **104**, 2043 (1996).
[63]F. W. Starr, F. Sciortino, and H. E. Stanley, "Dynamics of simulated water under pressure," Phys. Rev. E **60**, 6757 (1999).
[64]P. Crowther, F. Turci, and C. P. Royall, "The nature of geometric frustration in the Kob-Andersen mixture," J. Chem. Phys. **143**, 044503 (2015).
[65]J. F. Douglas and D. Leporini, "Obstruction model of the fractional Stokes–Einstein relation in glass-forming liquids," J. Non-Cryst. Solids **235**, 137 (1998).
[66]X. Xu, J. F. Douglas, and W.-S. Xu, "Parallel emergence of rigidity and collective motion in a family of simulated glass-forming polymer fluids," Macromolecules **56**, 4929 (2023).
[67]Q.-L. Yuan, X. Xu, J. F. Douglas, and W.-S. Xu, "Understanding relaxation in the Kob-Andersen liquid based on entropy, string, shoving, localization, and parabolic models," J. Phys. Chem. B **128**, 10999 (2024).
[68]E. R. Weeks, J. C. Crocker, A. C. Levitt, A. Schofield, and D. A. Weitz, "Three-dimensional direct imaging of structural relaxation near the colloidal glass transition," Science **287**, 627 (2000).
[69]P. Chaudhuri, L. Berthier, and W. Kob, "Universal nature of particle displacements close to glass and jamming transitions," Phys. Rev. Lett. **99**, 060604 (2007).
[70]B. Wang, S. M. Anthony, S. C. Bae, and S. Granick, "Anomalous yet Brownian," Proc. Natl. Acad. Sci. U. S. A. **106**, 15160 (2009).
[71]B. Wang, J. Kuo, S. C. Bae, and S. Granick, "When Brownian diffusion is not Gaussian," Nat. Mater. **11**, 481 (2012).
[72]E. Barkai and S. Burov, "Packets of diffusing particles exhibit universal exponential tails," Phys. Rev. Lett. **124**, 060603 (2020).
[73]H. Zhang, C. Zhong, J. F. Douglas, X. Wang, Q. Cao, D. Zhang, and J.-Z. Jiang, "Role of string-like collective atomic motion on diffusion and structural relaxation in glass forming Cu-Zr alloys," J. Chem. Phys. **142**, 164506 (2015).
[74]A. Heuer, "Information content of multitime correlation functions for the interpretation of structural relaxation in glass-forming systems," Phys. Rev. E **56**, 730 (1997).
[75]E. Flenner and G. Szamel, "Lifetime of dynamic heterogeneities in a binary Lennard-Jones mixture," Phys. Rev. E **70**, 052501 (2004).
[76]H. Mizuno and R. Yamamoto, "Lifetime of dynamical heterogeneity in a highly supercooled liquid," Phys. Rev. E **82**, 030501 (2010).
[77]R. K. Pandit and H. E. Castillo, "Simple model for dynamic heterogeneity in glass-forming liquids," Phys. Rev. Lett. **131**, 218202 (2023).
[78]Z. Song, C. Rodríguez-Tinoco, A. Mathew, and S. Napolitano, "Fast equilibration mechanisms in disordered materials mediated by slow liquid dynamics," Sci. Adv. **8**, eabm7154 (2022).
[79]R. P. White, S. Napolitano, and J. E. G. Lipson, "Mechanistic picture for the slow Arrhenius process in glass forming systems: The collective small displacements model," Phys. Rev. Lett. **134**, 098203 (2025).
[80]L. Ortlieb, T. S. Ingebrigtsen, J. E. Hallett, F. Turci, and C. P. Royall, "Probing excitations and cooperatively rearranging regions in deeply supercooled liquids," Nat. Commun. **14**, 2621 (2023).